Open Access
Full Paper

Journal of Agricultural Meteorology 80(1): 2–11, 2024

Special Collection: Agricultural Meteorology

Preferable weather patterns to brown planthopper advection to Kyushu and its effect of climate change

Keito Oishi[a], Masaru Inatsu[b,c,†] and Sho Kawazoe[b]

[a]Japan Meteorological Agency, 3–6–9 Toranomon, Minato, Tokyo 105–8431, Japan
[b]Faculty of Science, Hokkaido University, N10W8, Kita, Sapporo 060–0810, Japan
[c]Center for Natural Hazards Research, Hokkaido University, N9W9, Kita, Sapporo 060–8589, Japan

Abstract

The brown planthopper, *Nilaparvata lugens* (Stål), a type of rice pest, immigrates from southern China to western Japan by drifting in the southwesterly environment during the Baiu/Meiyu rainy season. This study aims to investigate the preferable weather patterns for the immigration of brown planthoppers across the East China Sea. We conducted immigration runs using an advection diffusion model for brown planthoppers and projected the possibility of them landing in Kyushu in the model run onto 64 weather map patterns typically observed in June and July, identified by the self-organizing map analysis. The results showed that the immigration occurred under two specific weather map patterns: flow stagnation around western Japan and a low-level jet blowing over the East China Sea. Consistency between landing cases in model runs and the occurrence of the two weather patterns was found in the intraseasonal and interannual variability. We also estimated the change in the frequency of brown planthopper arrival in Kyushu based on the climate change dataset, the database for Policy Decision Making for Future climate change (d4PDF). It was found that the flow stagnation patterns increased in response to global change, at least in the d4PDF dataset. Finally, risk assessment for temperature change and a comparison with trap observations were discussed.

Key words: Brown planthopper, Climate change, Weather patterns

1. Introduction

The brown planthopper *Nilaparvata lugens* (Stål), hereafter referred to as BPH, is one of the most destructive rice pests prevalent across the Asian-Australian monsoon region. Both nymphs and adults of BPH feed on plant sap from the base of tillers (Ghaffar *et al*., 2011; Prasad *et al*., 2009), which leads to hopperburn, a condition where rice leaves become brown and wilted. In addition, BPHs transmit two kinds of viruses that stunt growth (Cabacautan *et al*., 2009). Therefore, rice crops are seriously affected by large outbreaks of BPHs.

The BPHs overwinter not in Japan but in northern Vietnam (Takezawa, 1961; Okumura, 1963). They migrate to Southern China in spring and then fly across the East China Sea from June to July (Otuka *et al*., 2008). Kisimoto (1971) first found that the migration explained the trigger of BPH outbreaks in western Japan. Ohkubo (1973) supported his finding by conducting tethered flight tests to demonstrate the prolonged flying ability of BPHs in warm, moist conditions. Even if only a small number of BPHs settled down in paddy fields in Japan, a huge outbreak might occur due to a high fecundity rate and strong invasion ability. Commonly, the third generation after the migration causes damage to rice crops in early autumn (Matsumura *et al*., 2018; Tanaka *et al*., 2019). A key process of the outbreak is the breeding cycle is mostly controlled by temperature (Noda, 1989). The natural causes for BPH outbreaks are therefore the migration across the East China Sea and breeding across multiple generations, for which information may support the agricultural management by spraying the chemical pesticide (Zewen *et al*., 2003; Mao *et al*., 2019) at an appropriate timing to effectively kill nymphs in the first generation after the immigration (Powell *et al*., 1993).

The immigration and breeding of BPHs are both attributed to meteorological conditions related to the summertime Asian monsoon. Since the breeding depends primarily on accumulated temperature until autumn at the landing points, the possible number of generations can be easily estimated. It is well known that immigration is often successful when strong southwesterly wind, called low-level jet (Matsumoto, 1973), is observed in the Baiu-Meiyu rainy season. In fact, BPH immigration density was related to the number of days with a strong low-level jet over the East China Sea (Syobu *et al*., 2012). However, the variety of large-scale weather patterns that contribute to the immigration of BPHs have not been well documented. When considering the change in the summertime Asian monsoon due to global warming (Ose, 2019), the BPH immigration might be modulated by the increase or decrease in the preferable patterns.

A simulation model based on meteorological data is necessary to support the evaluation of the probability of BPH immigration. Otuka *et al*. (2005a) developed such a model that predicts the BPH movements by advection, diffusion, hovering at a temperature of 16.5 ℃ or higher (Ohkubo, 1973), and

Received; June 30, 2023
Accepted; December 3, 2023
†Corresponding author: inaz@sci.hokudai.ac.jp
DOI: 10.2480/agrmet.D-23-00022

taking-off from several points in southern China with continuous uplifting in an hour. The wet deposition was also considered recently (Otuka, 2018). The simulation results almost captured observation cases of BPH by moth traps or net traps at sites in western Japan, although the skill was hardly evaluated due to the difficulty of quantifying the spatial density of BPHs. The simulation system was implemented in the JPP-net member website (https://web1.jppn.ne.jp/member/) and is operated under the assumption that the BPHs take off from the points uniformly distributed over southern China and constantly in the season (Otuka *et al*., 2005b). Although the immigration simulation needs computational burden, the simulation cases could be reasonably selected in the weather pattern classification.

The purpose of this study is to investigate preferable weather patterns for the immigration of BPHs across the East China Sea. Whereas the low-level jet seems to be correlated with the possibility of immigration, it may not be the only weather pattern conducive for immigration. Climate change may primarily affect the BPH habitat through temperature changes, but it may also modulate the passage to western Japan through changes in weather patterns. It is also remarked that we here focused on one of the natural causes for BPH outbreaks in western Japan and excluded the effects of pesticides, plant diseases, natural enemies, and rice breed variety. We also ruled out other species of planthoppers than BPHs because the outbreak of the other species is too moderate to cause severe damage to rice crops in Japan. In this study, we use self-organizing maps (SOMs, Kohonen, 1995) to arrange the weather patterns based on the horizontal wind data within the planetary boundary layer, where BPHs are likely to hover. Moreover, we will project simulation results of the BPH immigration onto the SOMs. In Section 2, we will introduce the BPH simulation model and the SOMs used to classify the weather patterns around the East China Sea. Section 3 will demonstrate the consistency between the simulation results and the preferable weather pattern by SOMs. We will project the global-warming simulation results onto SOMs to identify the change in weather patterns. Section 4 discusses other possible agents related to global warming and some concerns about the simulation model.

2. Materials and methods

2.1 Datasets

The data used for BPH simulation and weather pattern classification were ERA5 reanalysis data provided by the European Centre for Medium-Range Weather Forecasts (Hersbach *et al*., 2021). This reanalysis data was arranged with a gridded configuration of 0.25° in longitude and 0.25° in latitude and provided at hourly intervals. The data were extracted from May to August between 2001 and 2020. We used a three-dimensional wind vector, air temperature, specific humidity, and geopotential height at finite vertical levels from 1000 hPa to 700 hPa and 10-m wind, 2-m temperature, 2-m dew point, surface pressure, sea level pressure, and total precipitation. The smoothed topography data accompanied by ERA5 were also utilized.

We used the database for Policy Decision Making for Future climate change (d4PDF, Mizuta *et al*., 2017; Fujita *et al*., 2019), which is a set of ensemble simulations with 60-km horizontal grid spacing of atmospheric general circulation model MRI-AGCM version 3.2, developed by Meteorological Research Institute (Mizuta *et al*., 2012). This data was only used for the preferable weather patterns to BPH landing because the resolution is insufficient to directly calculate BPH particles. The HIST experiment was conducted with greenhouse gas concentration and sea surface temperatures (SSTs) given as the historical records from 1951 to 2010. The NAT experiment was conducted with the pre-industrial level of greenhouse gas concentration and the same 1951−2010 SST data but detrended. The 2K and 4K experiments were conducted with the detrended SSTs added by climatological SST warming patterns from six models from phase 5 of the Coupled Model Intercomparison Project. The greenhouse gas concentration at the value of 2090 of representative concentration pathway 8.5 was given throughout the 60-year integration, and each pattern was multiplied by a scaling factor to give a global-mean surface air temperature warming of 2K or 4K. For saving computation, we selected six ensembles each from the HIST, NAT, 2K, and 4K experiments. For 2K and 4K, one ensemble from each of the six SST patterns was used.

2.2 BPH Immigration Model and Experiments

The BPH immigration model we used mostly followed Otuka *et al*. (2005a). The core component is a Lagrangian-type forward trajectory model that represents advection and turbulent mixing. Unlike Otuka *et al*. (2005a), we implemented horizontal diffusion and followed Gifford (1984) for vertical diffusion. We consider a representative BPH as an individual particle. The n-th particle's position $\boldsymbol{X}_n=(X_n, Y_n, Z_n)$ is updated every timestep Δt (10 min) following the formulation as

$$X_n(t+\Delta t)=X_n(t)+[U(\boldsymbol{X}_n, t)+u_n(t)]\,\Delta t, \quad (1)$$

$$Y_n(t+\Delta t)=Y_n(t)+[V(\boldsymbol{X}_n, t)+v_n(t)]\,\Delta t, \text{ and} \quad (2)$$

$$Z_n(t+\Delta t)=Z_n(t)+\left\{W(\boldsymbol{X}_n, t)+\frac{\partial K}{\partial z}(\boldsymbol{X}_n, t)+F\right\}\Delta t+\sqrt{24K\Delta t}\,G, \quad (3)$$

where (U, V, W) denotes three-dimensional wind vector, K is the vertical diffusion coefficient, G is a uniform random number ranging ± 0.5, and F is the initial rising rate as described below. The turbulent zonal and meridional winds (u_n, v_n) are updated by the first-order autoregression model with an autoregression coefficient of 0.988 s^{-1} and noise amplitude of 1.083 m s^{-1}. The wind vector, vertical diffusion coefficient, and vertical derivative are spatially interpolated from gridded reanalysis data on isobaric surfaces and just above the ground. We adopted the terrain following coordinate with the top height of 10 km.

The BPH particles take off at the initial time and then move upward with a rising velocity at 0.2 m s^{-1} in the first hour. We assume that, after rising, the BPHs only hover in temperatures above 16.5 ℃ against gravitational settling. As most of the BPHs are inactive below 16.5 ℃, the BPH particles cannot move to a higher altitude with the colder temperature. When the BPH particles go beyond the calculation domain from 100° E to 150° E and 5° N to 50° N, it is assumed that they become extinct. The

time integration stops at 24 hours after the take-off, because the BPHs attain their starvation survival time (Ohkubo, 1973). As the terminal velocity of the BPH was roughly estimated as 11 m s^{-1}, they are forced to land at the final position. The horizontal shift in the dropping can be ignored because the dropping from any height in the planetary boundary layer probably takes only a few minutes. We also incorporated the wet deposition process by causing particle extinction when the particle passes through areas with precipitation intensity exceeding 1 mm $hour^{-1}$.

The model was driven by atmospheric data based on ERA5. The integration timestep was 10 minutes. The BPHs take off at 10 UTC or 21 UTC every day from 1 June to 30 July; we set the take-off times corresponding to dusk and dawn at the local time following the observation (Ohkubo and Kisimoto, 1971). The number of flying BPHs was provided as a linear function between 13 ℃ and 26 ℃ of a temperature at the take-off point. The number above 26 ℃ is fixed at 1800 per flying event and zero below 13 ℃. The take-off points are distributed in southern China and Taiwan (Fig. 1) and initial points are given randomly in the 1° × 1° box of each take-off point.

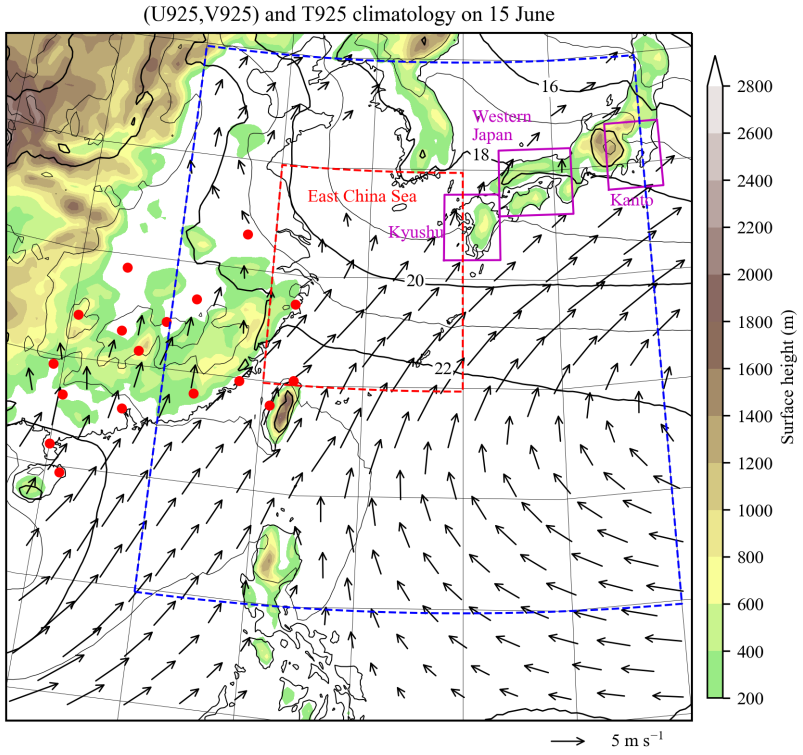

Fig. 1. Geographical map with surface height (m) shaded as per the reference on the right. Climatology at 925 hPa on the calendar date of 15 June is shown by contour for temperature with its interval being 1 K and is shown by vectors for horizontal wind with the reference of 5 m s^{-1} in the bottom. The vector of the wind magnitude less than 2 m s^{-1} is omitted. Red points denote the initial point where BPH takes off in the simulation. Box enclosed by magenta line shows the area where BPHs land on Kyushu, Western Japan, or Kanto, the box enclosed red dotted line shows the East China Sea area for temperature diagnosis, and the box enclosed blue dotted line shows the domain for combined EOF analysis.

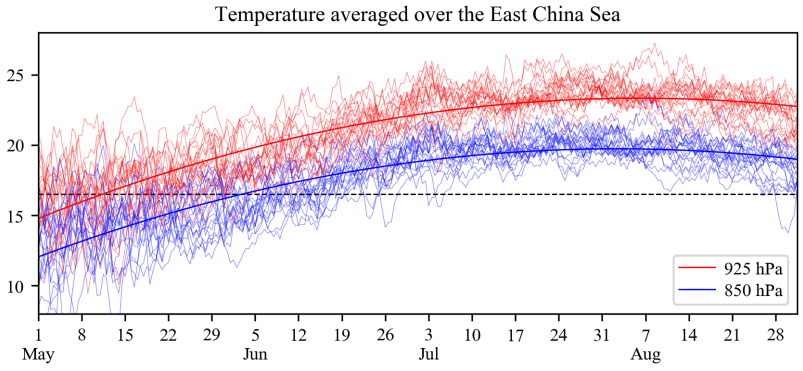

Fig. 2. Time series of air temperature (℃; red) at 925 hPa and (blue) at 850 hPa from May to August of each year between 2001 and 2020. Thick lines denote the climatology by fitting the mean value to a parabolic curve. The dotted line at 16.5 ℃ denotes the critical temperature for BPHs' hovering.

2.3 Weather Pattern Classification

The batch-learning SOM algorithm was trained on hourly horizontal wind anomalies at 925 hPa from a domain covering 115° E − 140° E by 15° N − 40° N (area enclosed by the dotted blue line in Fig. 1) in June and July from 2001 to 2020. The SOM configuration was an 8 × 8 node map[1]. We used a standard SOM algorithm with the Euclidean distance searching for the best matching unit. The dimension of input learning data was reduced by combined empirical orthogonal function (CEOF) for zonal and meridional winds without any adjustments to their magnitude. The composite map for a specific SOM node was made by averaging a climatic variable over the times identified as the node. The leading 60 CEOF modes that explained 80% of total variance were input to the SOM algorithm. The d4PDF simulation results were projected onto the SOM nodes by searching the nearest neighbor pattern from the reconstructed horizontal wind anomaly.

Here we remarked why we excluded temperature from the input of the SOM algorithm, despite previous weather pattern classifications by SOM in a similar domain (Ohba *et al*., 2015; Tamaki *et al*., 2018). As described in the BPH immigration model, BPHs initially rise to an altitude of 720 m (~ 925 hPa) above the ground, corresponding to the central altitude of the planetary boundary layer. Although the horizontal wind at this level mostly controls BPH immigration, the ceiling temperature of 16.5 ℃ limits the altitude of BPHs. However, the average temperature over the East China Sea (area enclosed by the dotted red line in Fig. 1) is higher than 16.5 ℃ at 925 hPa after mid-May and higher than it at 850 hPa after early June (Fig. 2). Considering the effect of vertical diffusion, BPHs are likely independent of the ceiling temperature in June and in July. Therefore, we classified weather patterns around the East China Sea based only on horizontal wind.

[1] The SOM map reduced to a smaller size like 5 × 5 forcibly placed clearly different patterns into a singular node. We decided to choose a SOM size of 8 × 8, enough to identify as many weather patterns as possible.

3. Results

3.1 Preferable Weather Patterns

Figure 3 displays the composite map of each SOM node for the analysis of the horizontal wind vector at 925 hPa, based on twice daily sampling between June and July from 2001 to 2020 using ERA5 reanalysis data (2,440 samples). The SOM map revealed several typical flow patterns in the planetary boundary layer during the summertime Asian monsoon season: The maps in the upper left corner showed the low-level jet over the East China Sea featuring warm-moist air intrusion and BPH immigration; the maps around #35 illustrated the flow stagnation in western Japan sandwiched between two high pressures; the maps on the right side detected the movement of a tropical cyclone; and the maps

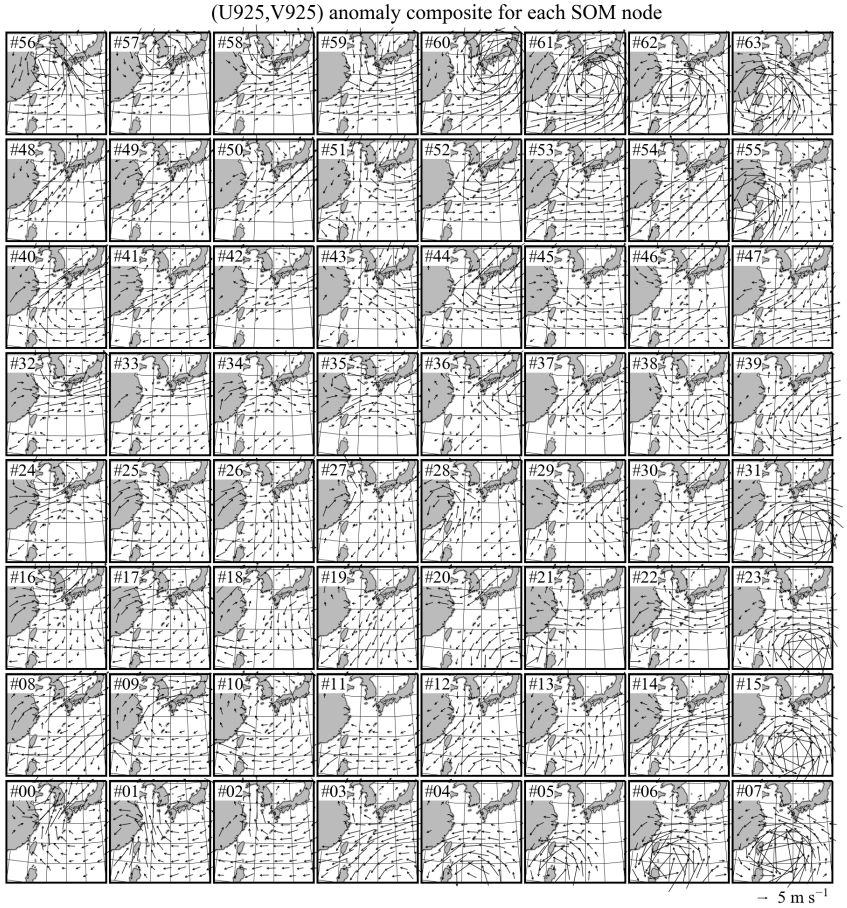

Fig. 3. Composite map of horizontal wind anomaly at 925 hPa for each SOM node computed for June and July from 2001 to 2020 based on ERA5 reanalysis data, with the reference of 5 m s^{-1} in the bottom right. The vector of the wind magnitude less than 2 m s^{-1} is omitted.

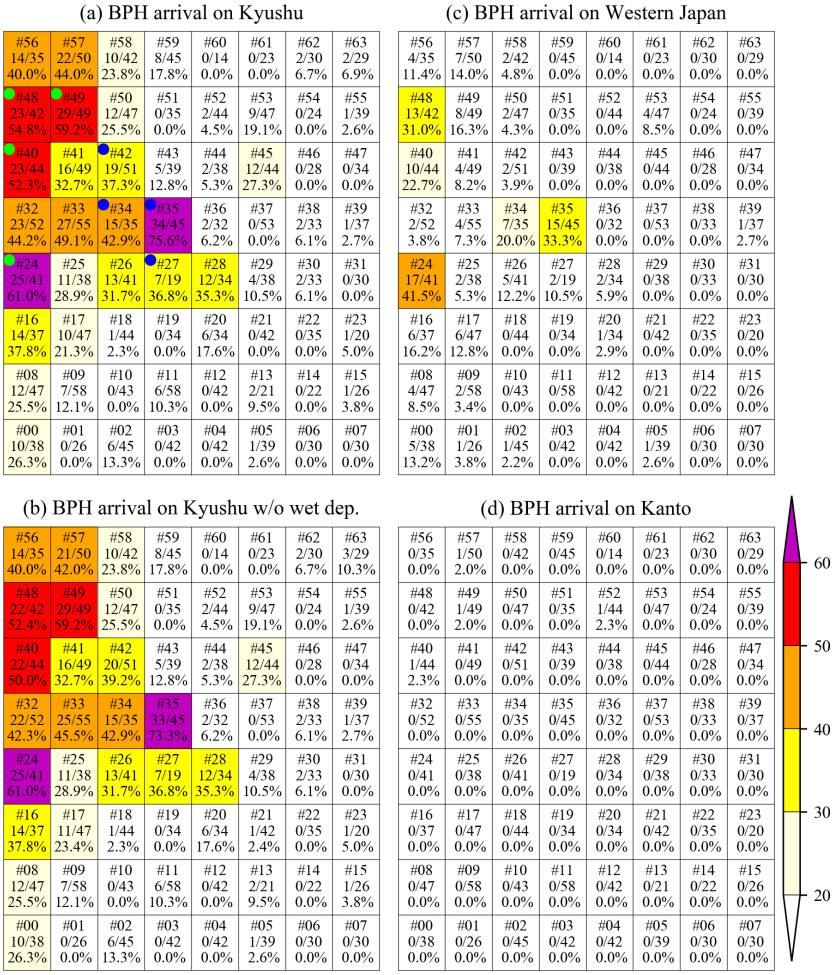

Fig. 4. (a, b) (Top line in each SOM) SOM node number, (middle) the number of cases where 90 or more BPH particles land in the areas of Kyushu area (area enclosed by the purple line in Fig. 1) in the simulation (a) with and (b) without wet deposition processes over the number of cases fallen into the SOM node, and (bottom) the ratio of BPH arrival to the total in the SOM node (%) filled with the color as the right reference. BPH simulations started from 10 UTC and 21 UTC correspond to SOM classifications at 12 UTC and 24 UTC, respectively. SOM nodes with blue and green marks denote groups A and B. (c, d) Same as Fig. 4a, but for the statistics for BPH particles landing on the areas of (c) western Japan and (d) Kanto areas.

in the bottom left showed the subtropical anticyclone covering Japan. The samples classified into each SOM node were almost uniformly distributed, with an average sample number of 38.1, ranging from 14 at #60 to 58 at #9 (Fig. 4).

The arrival of the BPH in the Kyushu area, defined as the BPH simulation cases where 90 or more representative particles landed within the domain of 129° E–132° E and 31° N–34° N (Fig. 4a), was observed to occur in the specific patterns among a variety of flow patterns classified by the SOM analysis (Fig. 3). The arrival probability in each SOM node was highest at #35 (75.6%) and second highest at #24 (61.0%; Fig. 4a). More than half of flow patterns at #40, #48, and #49 allowed for the BPH immigration. By examining the flow pattern difference in the SOM map, we identified two preferable weather patterns for the BPH immigration: group A with SOM nodes #27, #34, #35, and #42 and group B with SOM nodes #24, #40, #48, and #49[2]. Group A was closely related to the flow stagnation pattern in western Japan and characterized by two anticyclones residing in the southwest and north of Japan (Fig. 5a). In contrast, group B corresponded to the low-level jet with strong southwesterly winds blowing from Taiwan or southern China to western Japan (Fig. 5b). The result of BPH immigration is assumed to be mainly caused by horizontal advection because no substantial change can be found in the statistics based on the simulation without wet deposition processes (Fig. 4b). It is also noted that the direct arrival of the BPH in the western Japan (Fig. 4c) or Kanto areas (Fig. 4d) was rarely observed, compared to Kyushu case (Fig. 4a).

The annual appearance frequency of the two SOM groups defined above explained the interannual variability of the BPH arrival frequency in the simulation (Fig. 6). The appearance frequency of the preferable weather patterns, based on twice-daily sampling data in two months, averaged 16 samples and ranged from 3 to 33 samples. Although the BPH arrival frequency in the simulation was slightly higher than the appearance frequency of the preferable weather patterns, they were highly correlated, with correlation coefficients of 0.754 ($p<0.01$). The less

[2] The SOM nodes experiencing a high frequency of BPH landing can be categorized into three groups. However, this trial only added an intermediate weather pattern between Groups A and B (not shown).

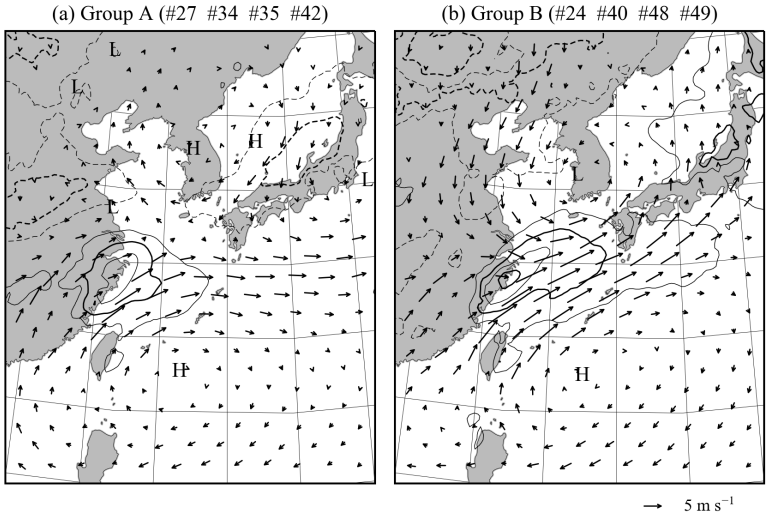

Fig. 5. The composite for (a) SOM group A (#27, #34, #35, and #42) and (b) SOM group B (#24, #40, #48, and #49). Vector shows horizontal wind anomaly at 925 hPa as the reference of 5 m s^{-1} in the bottom right. Contour shows temperature anomaly at 925 hPa with the interval being 0.5 K, negative contours dotted, and zero contour omitted. Marks of L and H respectively denote the local minimum and local maximum of sea level pressure anomaly.

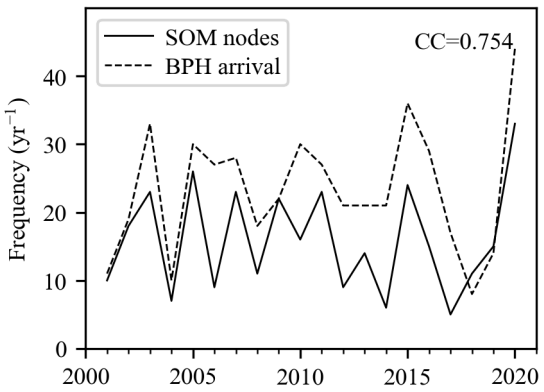

Fig. 6. Interannual variation of (solid line) frequency of samples (yr^{-1}) fallen into SOM groups A or B and (dashed line) frequency of days (yr^{-1}) when 90 or more BPH particles land on the Kyushu area in the simulation.

frequent feature in BPH arrivals to Kyushu Island was related to the difference in magnitude between June and July. Whereas the immigration simulation results were larger than the case for preferable weather patterns in June, they were lower in July (Fig. 7c). It should be noted that the flow stagnation in western Japan, group A in this study, was frequently observed from late June to early July (Fig. 7a), but the low-level jet over the East China Sea was constantly observed in June and July (Fig. 7b).

3.2 Projection to Climate Change

According to the d4PDF dataset, climate change has influenced the occurrence probability of weather patterns in northeast Asia during the Baiu/Meiyu season. The most significant change in the SOM map projection was the alternation of weather patterns associated with the tropical cyclone passage from the south (Fig. 8). Here, the HIST experiment is regarded as the reference because the probability distribution on the SOM map based on the ERA5 reanalysis data in 2001-2020 (Fig. 3) was almost reproduced by the experiment (not shown). The NAT experiment, which maintained greenhouse gas concentration at the pre-industrial levels, exhibited a higher frequency of patterns related to typhoon passage (Fig. 8a). On the other hand, the 2K and 4K experiments showed considerably low frequencies of such patterns (Figs. 8b, 8c). This finding is consistent with the previous global model studies, which have indicated a decrease in tropical cyclones in the western North Pacific due to increased stability in response to global warming, although some discrepancies exist (Knutson *et al*., 2010; Walsh *et al*., 2016; Yamada *et al*., 2017; Kawazoe *et al*., 2023).

The weather patterns that significantly influenced BPH immigration were also impacted by climate change. The SOM group A, associated with weather patterns characterized by the flow stagnation in western Japan (Fig. 6a), exhibited an increase due to global warming from late June to July (Fig. 7a). The frequency ratio of the NAT experiment to the HIST experiment was 0.88 during June and July, whereas the frequency ratio of the 4K experiment and the HIST experiment was 1.17. The frequency differences are statistically significant at a 1% level. On the other hand, the SOM group B, related to the weather patterns featuring a low-level jet over the East China Sea (Fig. 6b), experienced a slight decrease with a marginal significance level ($p<0.1$) in June due to global warming (Fig. 7b), which aligns with the findings of Ose (2019). Overall, the favorable weather patterns for the BPH immigration increased with higher greenhouse gas concentration levels, from the NAT experiment to the 4K experiment (Fig. 7c). The frequency increased by 3% (difference's $p<0.05$) in the 4K experiment compared to the HIST experiment. Due to the significant increase in the SOM group A, the increase in favorable weather patterns was 8% (difference's $p<0.05$) in July.

4. Discussion

4.1 Risk Assessment for Temperature Increase

The study demonstrated that the risk of BPH outbreaks in the Kyushu domain would increase in response to global

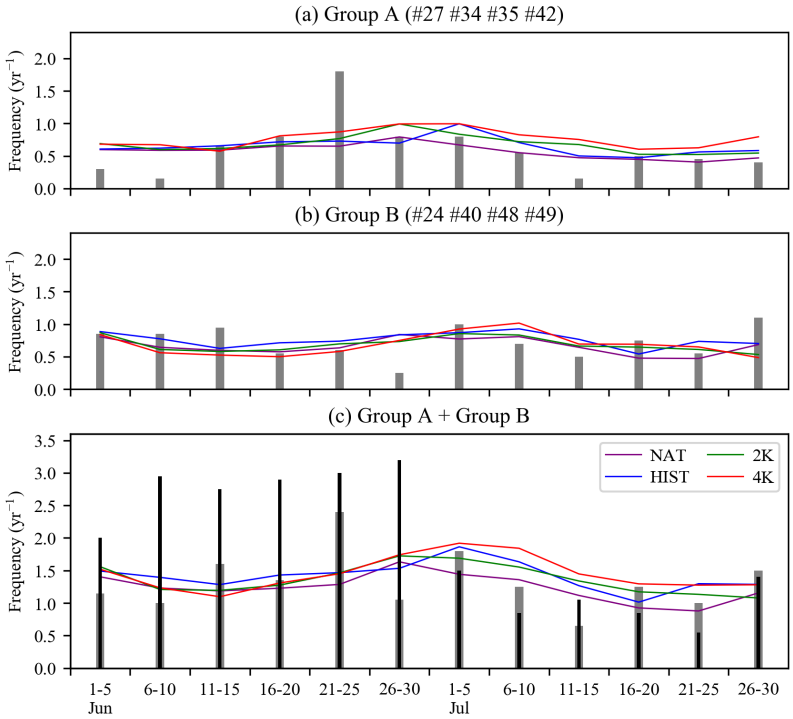

Fig. 7. Twice-daily statistics of frequency of days (yr^{-1}) fallen into (a) SOM group A, (b) SOM group B, and (c) SOM groups A and B in 6 ensembles of the d4PDF 60-yr simulation for (purple) NAT, (blue) HIST, (green) 2K, and (red) 4K experiments. The thick gray bar shows the SOM group frequency for ERA5 from 2001 to 2020 and the thin black bar in (c) shows the BPH arrival frequency in the simulation.

warming, particularly concerning BPH immigration over the East China Sea. Since BPH immigration is primarily influenced by horizontal winds in the planetary boundary layer, the impact of climate change is mostly limited to changes in weather patterns. However, the most significant change brought about by global warming is the rise in temperature, which unquestionably affects the BPHs' habitat. For instance, as previously indicated by Hu *et al*. (2015), the potential overwintering boundary may shift northward to central China in future climates. According to the d4PDF results, the 8 ℃ isothermal line at 925 hPa in January (Fig. 9), which corresponds to the 16 ℃ isothermal line at the surface, covered northern Vietnam in the HIST experiment. In the 4K experiment, this line shifted by 2 degrees north over the continent, allowing BPHs to overwinter even in southern China. This shift poses a greater threat not only to rice production in China by facilitating the breeding of more generations across larger crop areas but also to Japanese rice production by increasing the likelihood of direct immigration from the overwintering area. Another passage via the Korean Peninsula could also become more likely. Considering the counter-effect that nymphs of *N. lugens* currently inhabit temperatures close to their upper thermal limits, and the likelihood that increased temperatures would negatively impact their survival (Piyaphongkul *et al*., 2012), it can be inferred that the overwintering environment expands northward but does not necessarily become more favorable.

Another point in the BPH risk evaluation related to the temperature increase was the breeding cycle after landing on Kyushu Island. The BPHs stop growing below 12 ℃ and above 33 ℃, with the maximum development temperature at 28 ℃ (Syobu, 2002). Figure 10a illustrates the annual voltinism number on Kyushu Island, based on the ERA5 reanalysis, estimated by an effective cumulative temperature model with the baseline at 12 ℃, in which the immigrating generation lived in days with the cumulative temperature at 100 degree-days and the subsequential generations each spanned the days with the cumulative temperature at 398 degree-days. The BPHs were regarded to land on Kyushu Island if the preferable weather patterns occurred at the previous day. The estimated voltinisms from 2001 to 2020 equaled 2 with ~ 30% probability and 3 with ~ 60% probability, which was well reproduced by the HIST experiment (Fig. 10c). The voltinism number 3 after landing was the most possible from NAT (Fig. 10b), HIST and 2K (Fig. 10d). In contrast, the number decreased to 2 in the 4K experiment (Fig. 10e), because of the growing suppression by temperatures higher than 28 ℃ in boreal summer. The effect reduces the risk of BPH outbreaks in the Kyushu domain.

4.2 Comparison with Observations

We refrained from comparing the observations with simulation results in this paper because the observations using moth traps or net traps did not necessarily provide a quantitative estimate of the spatial density of BPH at any given time. However, the 20-year timeseries in our trial showed a moderate correspondence between the total number of trapped BPHs averaged over the observation sites in Kyushu Island obtained from the JPP-Net and the total number of simulated BPHs landing on the Kyushu domain in this study (Fig. 11). For example, our simulation indicated a small number of trapped BPHs in the seasons of 2001, 2004, and 2018, and a large number of trapped BPHs in the seasons of 2006 and 2020. The simulation did not accurately reproduce the timeseries of trapped BPHs in 2008 and 2011.

The mismatching in interannual variations between observation and simulation can be mostly attributed to the effects of pesticides. Spraying pesticides at the appropriate timing has proven effective in controlling BPH outbreaks in Japan, aided by a planthopper prediction system that takes atmospheric conditions into account (Syobu *et al.*, 2012). However, the continuous use of pesticides leads to the emergence of insects with pesticide resistance (Matsumura *et al.*, 2018). The continuous outbreaks of planthoppers since 2005 can be attributed to their susceptibility to pesticide (Fujii *et al.*, 2020). This indicates that the BPH risk assessment on the decadal scale must consider the development, dissemination, and overuse of planthopper pesticides.

The mismatching in daily variations between observation and simulation is likely due to the BPH immigration modeling. We speculate that the accuracy issue stems from the random and constant emission of BPHs over southern China. While no insect information was provided by China mainland, this issue could potentially be resolved through bilateral cooperation in pest damage control. Another problem in the simulation is the uniform treatment of BPH representative particles, despite Ohkubo's (1973) suggestion of a large discrepancy in BPH individuals. For instance, BPHs should cease hovering in environments colder than the ceiling temperature of 16.5 ℃, but one individual may stop at 13 ℃ while others may stop at 19 ℃. The time limitation for hovering also varies among BPH individuals. To improve simulation accuracy, we could introduce randomness in the ceiling temperature and hovering time. The issue of landing is also not

(a) NAT/HIST

#56 1.06	#57 1.05	#58 0.93	#59 0.89	#60 1.11	#61 1.15	#62 1.23	#63 1.06
#48 1.02	#49 0.94	#50 0.95	#51 1.40	#52 0.89	#53 0.87	#54 0.81	#55 1.09
#40 0.74	#41 0.82	#42 0.99	#43 0.97	#44 0.91	#45 0.90	#46 1.01	#47 0.98
#32 0.74	#33 0.88	#34 0.76	#35 0.80	#36 0.83	#37 1.12	#38 1.11	#39 1.07
#24 0.91	#25 0.72	#26 1.06	#27 0.89	#28 0.98	#29 0.96	#30 1.08	#31 1.46
#16 0.88	#17 0.83	#18 1.31	#19 1.20	#20 1.16	#21 1.38	#22 1.02	#23 1.29
#08 0.95	#09 0.88	#10 1.03	#11 0.98	#12 1.13	#13 1.25	#14 1.28	#15 1.31
#00 0.99	#01 1.01	#02 1.07	#03 1.16	#04 1.04	#05 1.21	#06 0.89	#07 1.18

(b) 2K/HIST

#56 0.85	#57 0.98	#58 1.35	#59 1.47	#60 1.10	#61 1.05	#62 0.98	#63 0.79
#48 0.98	#49 0.94	#50 0.95	#51 0.99	#52 1.03	#53 1.02	#54 0.78	#55 0.98
#40 0.77	#41 1.14	#42 1.07	#43 0.95	#44 1.12	#45 1.35	#46 1.17	#47 1.21
#32 1.07	#33 0.88	#34 1.06	#35 0.99	#36 0.88	#37 0.90	#38 0.96	#39 0.86
#24 1.04	#25 1.43	#26 1.18	#27 1.01	#28 0.87	#29 0.93	#30 1.00	#31 1.03
#16 1.12	#17 1.33	#18 1.19	#19 0.89	#20 0.66	#21 1.05	#22 0.93	#23 1.00
#08 0.93	#09 0.98	#10 1.02	#11 0.91	#12 0.94	#13 0.99	#14 0.78	#15 0.88
#00 0.91	#01 1.10	#02 0.97	#03 0.87	#04 0.88	#05 0.91	#06 0.69	#07 0.77

(c) 4K/HIST

#56 0.64	#57 0.92	#58 1.70	#59 1.91	#60 1.16	#61 0.99	#62 0.78	#63 0.42
#48 1.06	#49 0.90	#50 0.60	#51 0.75	#52 0.91	#53 1.70	#54 1.10	#55 0.77
#40 0.61	#41 1.63	#42 1.14	#43 0.97	#44 1.40	#45 2.53	#46 1.23	#47 1.92
#32 0.90	#33 0.67	#34 1.15	#35 1.18	#36 0.52	#37 0.75	#38 0.91	#39 1.16
#24 1.32	#25 2.43	#26 1.87	#27 1.25	#28 0.77	#29 1.02	#30 1.26	#31 0.63
#16 1.34	#17 1.48	#18 1.55	#19 0.76	#20 0.35	#21 0.78	#22 0.64	#23 0.47
#08 0.94	#09 0.77	#10 0.69	#11 0.56	#12 0.27	#13 0.46	#14 0.53	#15 0.52
#00 0.75	#01 0.83	#02 0.71	#03 0.41	#04 0.50	#05 0.44	#06 0.50	#07 0.47

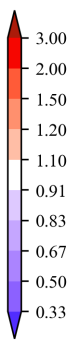

Fig. 8. The frequency ratio to HIST experiment of (a) NAT, (b) 2K, and (c) 4K experiments in each SOM node, colored as per the reference in the bottom right.

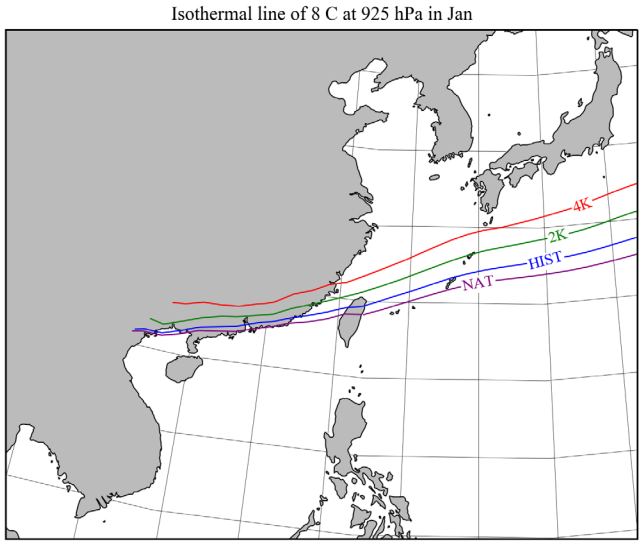

Fig. 9. Isothermal line at 8 ℃ of climatological temperature at 925 hPa in January for (purple) NAT, (blue) HIST, (green) 2K, and (red) 4K experiments.

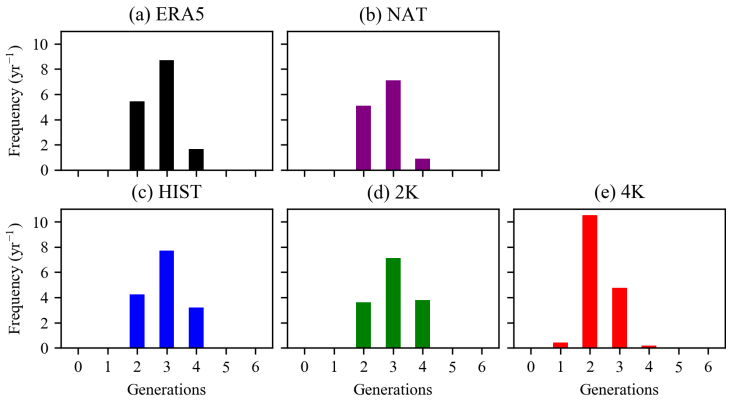

Fig. 10. Histogram of generation frequency (yr^{-1}) after landing on Kyushu estimated by accumulated temperature models with the twice-daily statistics (a) based on the ERA5 reanalysis data and based on (b) NAT, (c) HIST, (d) 2K, and (e) 4K experiments.

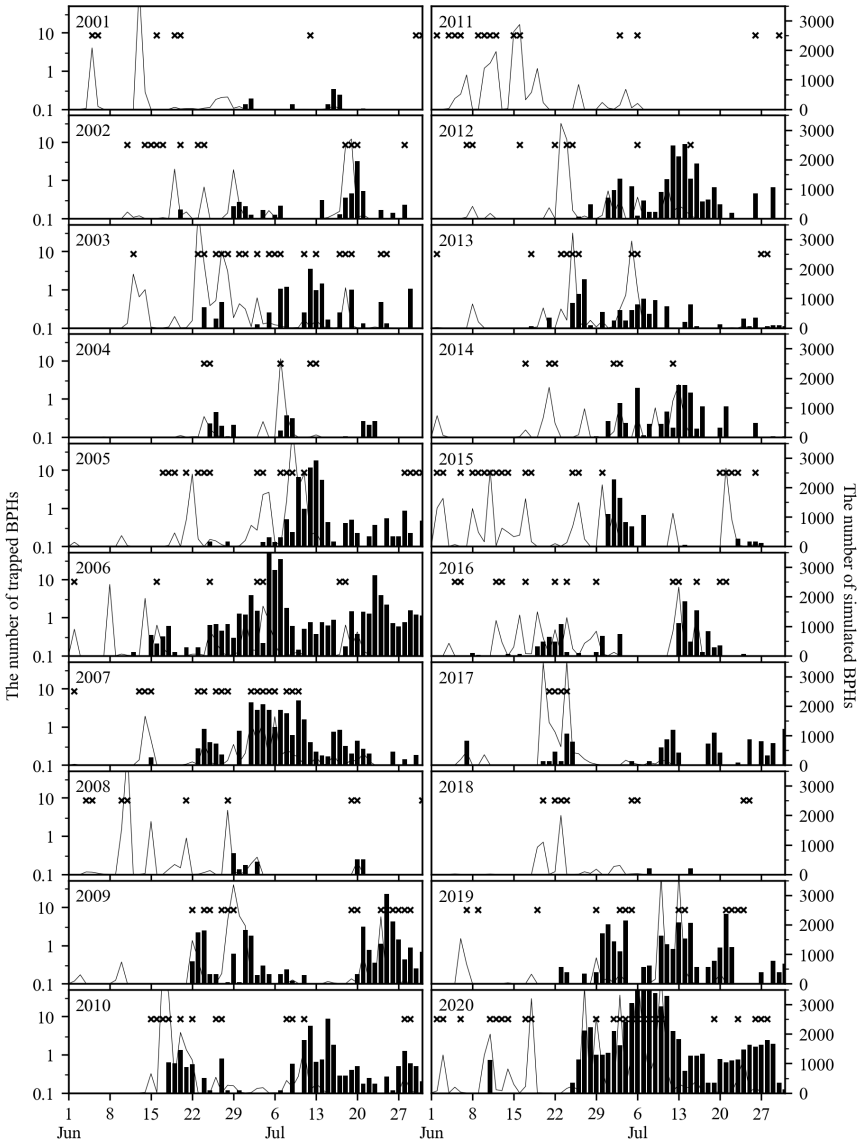

Fig. 11. Time series from 2001 to 2020 of (bar; left axis) the number of trapped BPHs averaged over sites in Kyushu Island, (line; right axis) the number of BPHs landing on the Kyushu domain in the simulation, and (cross marks) preferable weather patterns in the previous days.

well understood. In this simulation, we consider a successful landing when BPHs reside at an altitude lower than 100 m. However, there is no scientific basis for this treatment. Landing may be influenced by small-scale orography and associated downhill flow, which cannot be adequately resolved using low-resolution atmospheric data. Dynamical downscaling to a few kilometer scales could potentially alleviate this problem.

Acknowledgments

We would like to thank Dr. Akira Otuka, who advised the numerical simulation, and Prof. Tomoyoshi Hirota, Dr. Shinichiro Syobu, and Dr. Sachiko Matsumoto, who gave us insightful comments related to our earlier works. MI was financially supported by JSPS KAKAENHI (19H00963), by JPMXD0722680734 of the Ministry of Education, Sports, Culture, Science and Technology (MEXT), and by Research Field of Hokkaido Weather Forecast and Technology Development (endowed by Hokkaido Weather Technology Center Co. Ltd.).

References

Cabacautan PQ, Cabunagan RC, Choi IR, 2009: Rice viruses transmitted by the brown planthopper Nilaparvata lugens Stål. *Planthoppers: new threats to the sustainability of intensive rice production systems in Asia* (Heong KL, Hardy B, Ed.) Los Baños, the Philippines. 357–368.

Fujii T, Sanada-Morimura S, Oe T *et al*., 2020: Long-term field insecticide susceptibility data and laboratory experiments reveal evidence for cross resistance to other neonicotinoids in the imidacloprid-resistant brown planthopper Nilaparvata lugens. *Pest Management Science* **76**, 480–486.

Fujita M, Mizuta R, Ishii M *et al*., 2019: Precipitation changes in a climate with 2-K surface warming from large ensemble simulations using 60-km global and 20-km regional atmospheric models. *Geophysical Research Letters* **46**, 435–442.

Ghaffar MBAB, Pritchard J, Lloyd BF, 2011: Brown planthopper (*N. lugens Stal*) feeding behaviour on rice germplasm as an indicator of resistance. *Plos One* **6**, 1–13.

Gifford FA, 1984: The random force theory: Application to

meso- and large-scale atmospheric diffusion. *Boundary-Layer Meteorology* **30**, 159–175.

Hersbach H, Bell B, Berrisford P *et al*., 2021: The ERA5 global reanalysis. *Quarterly Journal of Royal Meteorological Society* **147**, 1956–1991.

Hu C, Hou M, Wei G *et al*., 2015: Potential overwintering boundary and voltinism changes in the brown planthopper, *Nilaparvata lugens*, in China in response to global warming. *Climatic Change* **132**, 337–352.

Kawazoe S, Inatsu M, Yamada TJ *et al*., 2023: Future changes in tropical and extratropical cyclones affecting Hokkaido and their related precipitation based on large-ensemble climate simulations, *Journal of Applied Meteorology and Climatology* **62**, 341–359.

Kisimoto R, 1971: Long distance migration of planthoppers, *Sogatella furcifera and Nilaparvata lugens. Symposium on Rice Insects Tropical Agricultural Research Series* **5**, 201–216.

Knutson TR, McBride JL, Chan J *et al*., 2010: Tropical cyclones and climate change. *Nature Geoscience* **3**, 157–163.

Kohonen T, 1995: Self-organizing maps. *Springer Series in Information Sciences*, Vol. 30, Springer-Verlag, 362 pp.

Mao K, Zhang X, Ali E *et al*., 2019: Characterization of nitenpyram resistance in *Nilaparvata lugens* (Stål). *Pesticide Biochemistry and Physiology* **157**, 26–32.

Matsumoto S, 1973: Lower tropospheric wind speed and precipitation activity. *Journal of Meteorological Society of Japan* **51**, 101–107.

Matsumura M, Sanada-Morimura S, Otuka A *et al*., 2018: Insecticide susceptibilities of the two rice planthoppers *Nilaparvata lugens* and *Sogatella furcifera* in East Asia, the Red River Delta, and the Mekong Delta. *Pest Management Science* **74**, 456–464.

Mizuta R, Yoshimura H, Murakami H *et al*., 2012: Climate simulations using MRI-AGCM 3.2 with 20-km grid. *Journal of Meteorological Society of Japan* **90**, 233–258.

Mizuta R, Murata A, Ishii M *et al*., 2017: Over 5,000 years of ensemble future climate simulations by 60-km global and 20-km regional atmospheric models. *Bulletin of American Meteorological Society* **98**, 1383–1398.

Noda H, 1989: Developmental zero and total effective temperature of three rice planthoppers (Homoptera: Delphacidae). *Japanese Journal of Applied Entomology and Zoology* **33**, 263–266.

Ohba M, Kadokura S, Yoshida Y *et al*., 2015: Anomalous weather patterns in relation to heavy precipitation events in Japan during the baiu season. *Journal of Hydrometeorology* **16**, 688–701.

Ohkubo N, Kisimoto R, 1971: Diurnal periodicity of flight behaviour of the brown planthopper, Nilaparvata lugens Stål, in the 4th and 5th emergence periods. *Japanese Journal of Applied Entomology and Zoology* **15**, 8–16 (in Japanese with English summary).

Ohkubo N, 1973: Experimental studies on the flight of planthoppers by the tethered flight technique. *Japan Journal of Applied Entomology and Zoology* **17**, 10–18 (in Japanese with English summary).

Okumura T, 1963: Induction of diapause in eggs of the planthoppers, *Sogata furcifera* and *Nilaparvata lugens* by changing rearing condition of their adult life. *Japan Journal of Applied Entomology and Zoology* **7**, 285–290.

Ose T, 2019: Characteristics of future changes in summertime East Asian monthly precipitation in MRI-AGCM global warming experiments. *Journal of Meteorological Society of Japan* **97**, 317–335.

Otuka A, Dudhia J, Watanabe T *et al*., 2005a: A new trajectory analysis method for migratory planthoppers, *Sogatella furcifera* (Horváth) (Homoptera: Delphacidae) and *Nilaparvata lugens* (Stål), using an advanced weather forecast model. *Agricultual and Forest Entomology* **7**, 1–9.

Otuka A, Watanabe T, Suzuki Y *et al*., 2005b: Real-time prediction system for migration of rice planthoppers *Sogatella furcifera* (Horváth) and *Nilaparvata lugens* (Stål) (Homoptera: Delphacidae). *Applied Entomology and Zoology* **40**, 221–229.

Otuka A, Matsumura M, Watanabe T *et al*., 2008: A migration analysis for rice planthoppers, *Sogatella furcifera* (Horváth) and *Nilaparvata lugens (Stål)* (Homoptera: Delphacidae), emigrating from northern Vietnam from April to May. *Applied Entomology and Zoology* **43**, 527–534.

Otuka A, 2018: Migration analyses and predictions for migratory insect pests toward Japan. Proceedings of the 2018 International Symposium on Proactive Technologies for Enhancement of Integrated Pest Management of Key Crops. 103–119.

Piyaphongkul J, Pritchard J, Bale J, 2012: Heat stress impedes development and lowers fecundity of the brown planthopper *Nilaparvata lugens* (Stål). *PLoS One* **7**, e47413. doi:10.1371/journal.pone.0047413.

Powell KS, Gatehouse AMR, Hilder VA *et al*., 1993: Antimetabolic effects of plant lectins and plant and fungal enzymes on the nymphal stages of two important rice pests, *Nilaparvata lugens* and *Nephotettix cinciteps*. *Entomologia Experimentalis et Applicat* **66**, 119–126.

Prasad GSV, Sastry MVS, Rao JRK *et al*., 2009: Relationships of brown planthopper resistance to tungro virus and grain characteristics in rice. *The Journal of Agricultural Science* **109**, 609–610.

Syobu S, 2002: Improvements in the forecasting techniques of rice planthopper occurrence. *Plant Protection* **56**, 474–478.

Syobu S, Otuka A, Matsumura M, 2012: Annual fluctuations in the immigrant density of rice planthoppers, *Sogatella furcifera* and *Nilaparvata lugens* (Hemiptera: Delphacidae), in the Kyushu district of Japan, and associated meteorological conditions. *Applied Entomology and Zoology* **47**, 399–412.

Takezawa H, 1961: Studies on the overwintering of the brown planthopper, *Nilaparvata lugens Stål.* I. Overwintering of the brown planthopper egg under the natural temperature condition. *Japan Journal of Applied Entomology and Zoology* **5**, 40–45.

Tamaki Y, Inatsu M, Dzung NL *et al*., 2018: Heavy-rainfall duration bias in dynamical downscaling and its related synoptic patterns in summertime Asian monsoon. *Journal of Applied Meteorology and Climatology* **57**, 1477–1496.

Tanaka K, Otuka A, Matsumura M, 2019: Generation forecast of *Nilaparvata lugens* using forecast data of agrometeorological grid square data system. *Kyushu Plant Protection Research* **65**, 75–83.

Walsh KJE, McBride JL, Klotzbach PJ *et al*., 2016: Tropical cyclone and climate change. *Wiley Interdisciplinary Reviews Climate Change* **7**, 65–89, doi:10.1002/wcc.371.

Yamada Y, Satoh M, Sugi M *et al*., 2017: Response of tropical cyclone activity and structure to global warming in a high-resolution global nonhydrostatic model. *Journal of Climate* **30**, 9703–9724

Zewen L, Zhaojun H, Yinchang W *et al*., 2003: Selection for imidacloprid resistance in *Nilaparvata lugens*: cross-resistance patterns and possible mechanisms. *Pest Management Science* **59**, 1355–1359.